ACS Catalysis

pubs.acs.org/acscatalysis Research Article

Discovery of UbiA-Type Cyathane Synthases in Bacteria

Tyler A. Alsup, Diana P. Łomowska-Keehner, Melvin Osei Opoku, Zining Li, Caitlin A. McCadden, Tracy Qu, Glen Gillia, Jordan Nafie, and Jeffrey D. Rudolf*

Cite This: ACS Catal. 2025, 15, 16873−16881 Read Online

ACCESS | Metrics & More | Article Recommendations | Supporting Information

ABSTRACT: UbiA-type terpene synthases, traditionally annotated as prenyltransferases, have been shown to catalyze terpene cyclization in recent years, expanding their catalytic repertoire beyond primary metabolism. Here, we report on the genome-guided discovery and functional characterization of bacterial UbiA diterpene synthases (diTSs). Using a geranylgeranyl diphosphate (GGPP)-overproducing *Escherichia coli* system, we screened 32 candidate enzymes and identified five that generate structurally diverse diterpenes, two of which represent bacterial examples of cyathane synthases. Site-directed mutagenesis uncovered active-site residues that influence product formation, directing cyclization toward mono- or tricyclic products. This study expands the known catalytic repertoire of UbiA enzymes and highlights their untapped potential in bacterial terpenoid biosynthesis. Our findings suggest that bacteria may produce diverse and bioactive diterpenoids using UbiA TSs for the first committed biosynthetic step, warranting further exploration of UbiA TSs for natural product discovery.

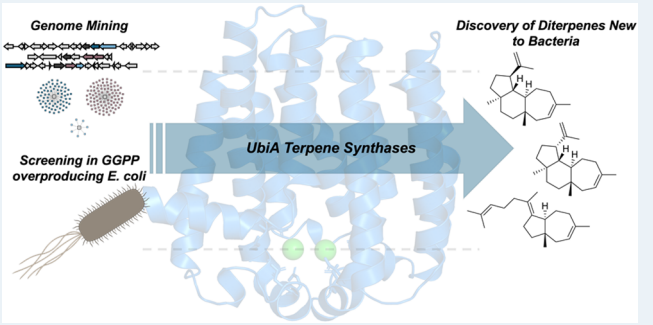

KEYWORDS: *diterpene synthase, cyathane, terpenoid, UbiA, vibrational circular dichroism*

INTRODUCTION

The structurally and stereochemically complex hydrocarbon skeletons of terpenoid natural products (NPs) are created from acyclic, achiral polyprenyl (C_{5n}) diphosphates by terpene synthases (TSs). TSs are represented by two canonical classes, type I and type II, that are differentiated based on how they initiate cyclization.[1,2] These mesmerizing enzymes are often the first committed step in the biosynthesis of the >100,000 terpenoid NPs known in nature.[3−6] Bacteria, even though they are often overlooked as terpenoid producers,[7−9] have a vast genetic repertoire for terpene biosynthesis that includes both classes of canonical TSs as well as several families of noncanonical TSs.[10] Very recently, we reported a large genome-based screen for canonical type I diterpene synthases (diTSs) from bacteria resulting in a high percentage of hits and the identification of several novel diterpene skeletons from a variety of bacteria, as well as diterpenes that were only previously known in other, nonbacterial, organisms.[8] We wanted to extend this exploratory diterpene screen to UbiA-type TSs from bacteria.

UbiA prenyltransferases (PTs) are transmembrane proteins that are integral in the biosynthesis of ubiquinones, menaquinones, vitamins, porphyrins, and structural components of cell membranes across all domains of life.[11,12] The UbiA superfamily of enzymes, historically thought to exclusively catalyze prenyl transfer reactions, were shown in recent years to be capable of terpene cyclization.[13−16] From a chemical and structural perspective, this is logical as both PTs and type I TSs require carbocations generated via diphosphate abstraction, have bipartite active sites with conserved Asp rich motifs (NQxx(G/A)xxxD and DxxDxxxD in UbiA TSs) and a large hydrophobic pocket to accommodate the polyprenyl diphosphate substrates, and fold into similar α-helical structures. The first examples of bacterial UbiA TSs were established in the platencin biosynthetic pathway, where PtmT1/PtnT1 form *ent*-atiserene from *ent*-copalyl diphosphate.[13] The first characterized fungal UbiA TS was *fma*-TC, a sesquiterpene synthase responsible for forming the *trans*-bergamotene core of fumagillin.[15] Since then, several studies followed with examples capable of forming (poly)cyclic sesquiterpene, diterpene, and sesterterpene skeletons.[14,16,17]

In this study, we employed genome mining to identify and characterize putative UbiA-type diTSs in bacteria. After prioritizing putative UbiA TSs by distinguishing between those likely involved in primary and secondary metabolism, we used an engineered *Escherichia coli* diterpene production system to screen 32 putative TSs. We characterized five UbiA diTSs. Two quite distinct TSs form diastereomers of the

Received: July 7, 2025
Revised: September 15, 2025
Accepted: September 16, 2025
Published: September 22, 2025

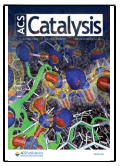

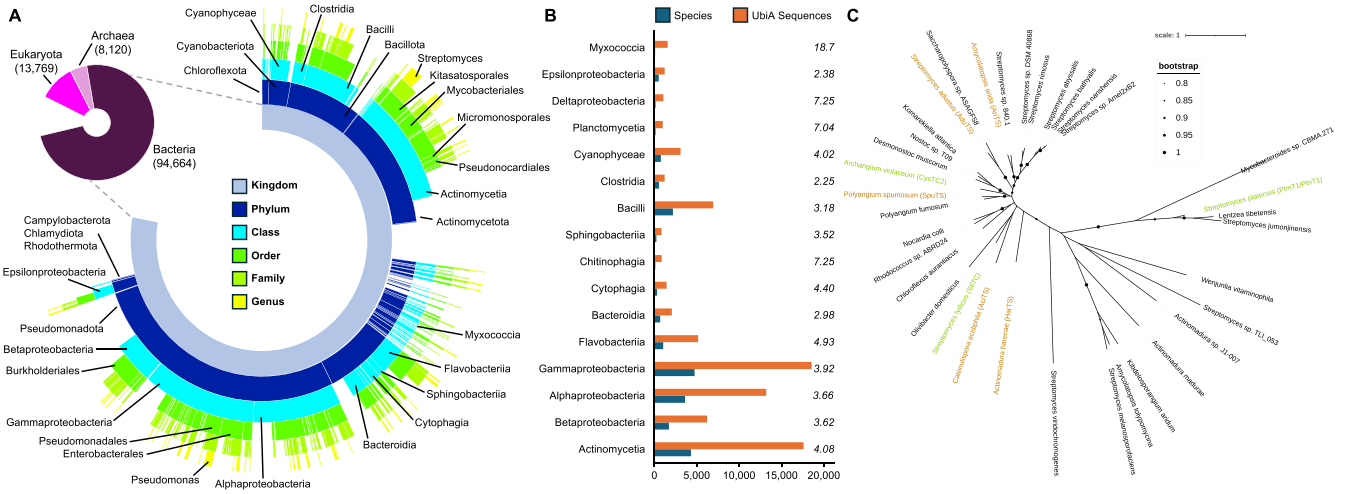

Figure 1. Bioinformatic exploration of the UbiA superfamily (IPR044878) in bacteria. (A) Sunburst diagram highlighting the phylogenetic breakdown of UbiA superfamily members across 39 bacterial phyla. Selected taxonomic descriptions are given. (B) Comparison of total UbiA enzymes per number of species for selected bacterial classes. Averages are given for each class. (C) Unrooted maximum likelihood phylogenetic tree of 32 UbiAs screened in this study and previously characterized bacterial UbiA diTSs StlTC, CysTC2, and PtmT1/PtnT1.

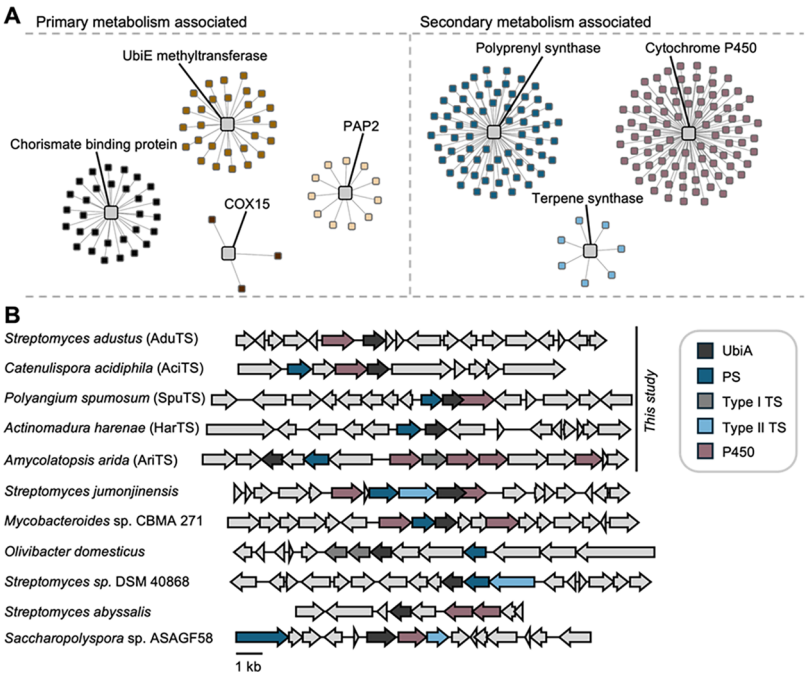

Figure 2. Genome mining of UbiA TSs from bacteria. (A) Subset of a UbiA genome neighborhood diagram highlighting selected protein families involved in primary and secondary metabolism. (B) Diverse UbiA-harboring biosynthetic gene clusters identified in this work.

7/6/5-tricyclic cyathane skeleton; these are the first cyathane TSs from bacteria. We also identified a TS that builds the 5/7-bicyclic isopseudolaratriene, a skeleton that has only been seen in plants. Molecular docking and mutational studies revealed insights into UbiA TS enzymology and serve as a foundation for future mechanistic exploration.

RESULTS AND DISCUSSION

Genome Mining for Bacterial UbiA-like Terpene Synthases. With a relatively small number of functionally characterized UbiA TSs in bacteria, their roles in specialized metabolism remain largely unknown. In bacteria, there are eight functionally characterized UbiA TSs;[13,16,17] in comparison, there are >180 characterized canonical type I TSs.[8] Of the 241 terpenoid biosynthetic gene clusters (BGCs) in the MIBiG database,[18] only 24 include UbiA-type enzymes, 19 of which are PTs and five are TSs (Figure S1), underscoring the gap in exploration of these enzymes in secondary metabolism. Genome mining efforts have largely overlooked this class of TSs due to the assumption that UbiA enzymes are predominantly involved in primary metabolism or are simply PTs.[11] The membrane-bound nature of UbiA enzymes poses additional challenges in the preparation of protein for in vitro characterization, a strategy that is routine with canonical TSs. We previously showed that an engineered *E. coli* strain that overproduces geranylgeranyl diphosphate (GGPP) could be readily used to characterize the function of UbiA TSs without the need for protein purification and in vitro studies.[19] With

https://doi.org/10.1021/acscatal.5c04650
ACS Catal. 2025, 15, 16873−16881

this system in hand, we set out to screen a library of putative UbiA TSs from bacteria.

We were first curious about the prevalence of UbiA enzymes (IPR044878) in bacteria. In the InterPro database, >94,000 sequences were from bacteria, outnumbering those from Eukaryota (>13,700) and Archaea (>8100). Further taxonomic separation of the bacterial hits revealed Actinomycetota and Pseudomonadota as significant reservoirs of putative UbiA enzymes in the public repositories (Figure 1). A comparison of total UbiA enzymes per number of species revealed an average of 4.2 UbiA enzymes in Bacteria and Eukaryota and 5.6 in Archaea. It should be noted that classes within the Actinomycetota and Pseudomonadota phyla averaged 3.6−4.1 UbiAs per species, some classes had more on average, e.g., Chitinophagia and Planctomycetia had >7 (Figure 1), despite these species being underrepresented in the InterPro database; Myxococcia had >18, but this outlier is likely due to its relatively smaller numbers of classified phylogenetic species. These observations, along with Actinomycetota being well-known producers of natural products[20,21] and harborers of canonical TSs,[8,9,22] support that actinomycetes are an ideal source for the discovery of UbiA-type TSs.

To prioritize candidates for screening, we aimed to distinguish UbiA enzymes involved in primary and secondary metabolism. Using the >18,000 members of the UbiA superfamily from actinomycetes, we generated a sequence similarity network (SSN) using the Enzyme Function Initiative webtools.[23] At an e-value of 10^{-65}, large subfamilies of UbiA PTs were observed and annotated based on homologies to known enzymes in primary metabolism; smaller clusters and singletons were annotated based on their InterPro designations (Figures S2 and S3). Because the majority these proteins are proposed to be PTs, we created a genome neighborhood network (GNN) of this SSN to assess which UbiAs were found in genetic proximity to conserved primary metabolism genes (Figure 2A). For example, UbiA members encoded near a 1,4-dihydroxy-2-naphthoate synthase (UbiE; PF01209) would likely act together in menaquinone biosynthesis.[11,12] Following similar logic for other well-known primary metabolic pathways involving UbiA PTs, we observed clustering with genes encoding cytochrome oxidase assembly proteins (Cox15; PF02628), chorismate binding proteins (CBP; PF00425), and phosphatidic acid phosphatases (PAP2; PF01569), proteins involved in the biosyntheses of hemes, *para*-hydroxybenzoic acid, and digeranylgeranylglycerol phosphate.[11] Conversely, we searched for UbiAs that were clustered with polyprenyl synthases (PPS; PF00348), cytochromes P450 (P450; PF00067), or other TSs (PF19086) as they are commonly involved in the biosynthesis of terpenoid NPs.[3,5,24] Several BGCs included multiple P450s suggestive of highly oxidized terpenoids while others included type II TSs (Figure 2B), reminiscent of the platencin BGC.[13] We thus prioritized putative UbiA TSs for discovery efforts based on the presence of at least one PPS, P450, or TS gene and no discernible UbiE, Cox15, CBP, or PAP2 genes. While the majority of UbiAs selected were from actinomycetes, we applied this genome mining approach to also include a few selected UbiAs from other nonactinomycete bacteria.

Discovery of the First Cyathane Diterpenes from Bacteria. Based on the bioinformatic prioritization described above, we synthesized 32 codon-optimized UbiA genes for expression in *E. coli*. Each gene was individually expressed in our GGPP-overproducing *E. coli* system[25] and diterpene products were initially detected by HPLC analysis. Seven positive hits (21%) were identified, including the positive controls CysTC2 from *Archangium violaceum* and StlTC from *Streptomyces lydicus* (Figure 3).[16] We scaled up fermentations

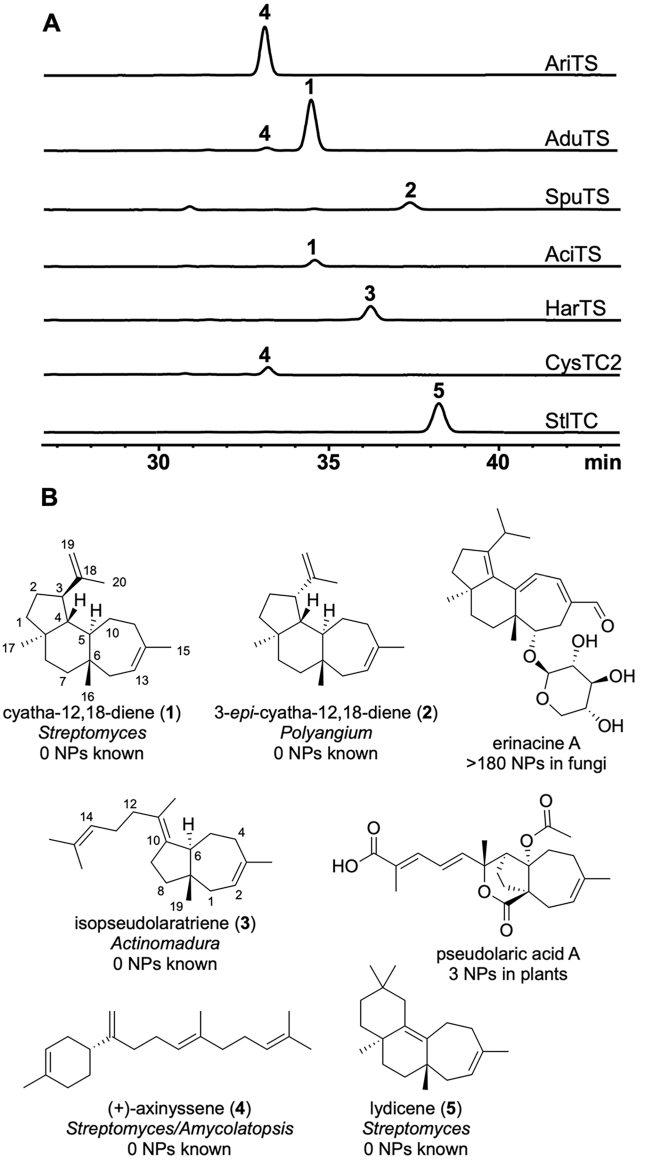

Figure 3. Diterpenes isolated from UbiA diTSs in this study. (A) HPLC-UV analysis (210 nm) of extracts obtained from expressing UbiAs in our GGPP-overproducing *E. coli* strain. (B) Structures of compounds **1**−**4** isolated from UbiA TSs and previously reported natural products originating from similar diterpene skeletons.

of the five other hits, AriTS from *Amycolatopsis arida*, AduTS from *Streptomyces adustus*, SpuTS from *Polyangium spumosum*, AciTS from *Catenulispora acidiphila*, and HarTS from *Actinomadura harenae*, for product isolation and structural elucidation (Table S1). We isolated diterpenes **1**−**4** and determined their structures using comprehensive NMR, GC-MS, and vibrational circular dichroism (VCD) analyses.

Cyatha-12,18-diene (**1**), a diterpene newly identified from bacteria but previously isolated from the sponge *Higginsia* sp.,[26] was produced by the UbiA TSs AduTS from *S. adustus* and AciTS from *C. acidiphila* (Figure 3). The EIMS of **1** showed a molecular ion peak at *m*/*z* 272.2 (Figure S4; high-

https://doi.org/10.1021/acscatal.5c04650
ACS Catal. 2025, 15, 16873−16881

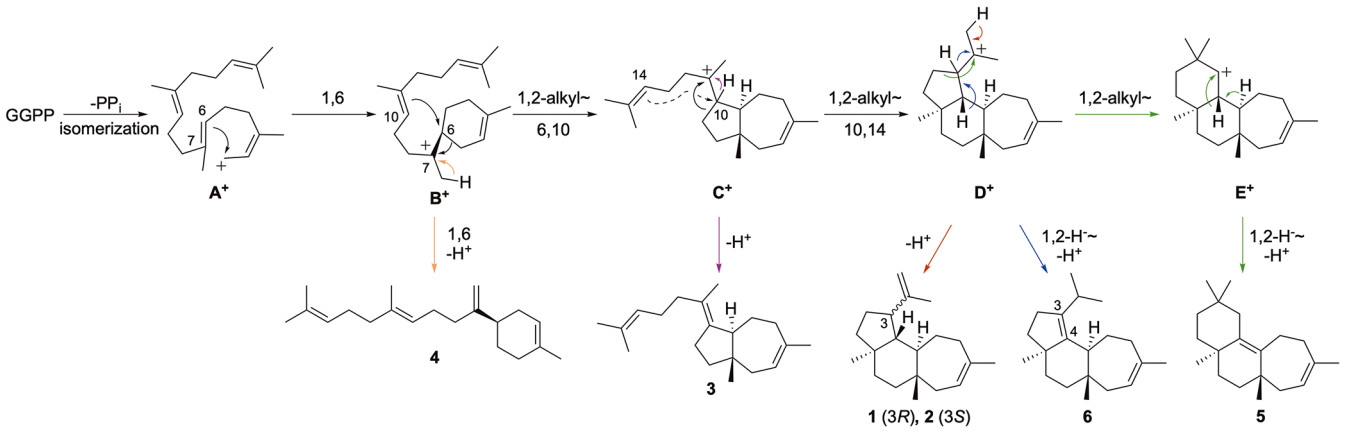

Figure 4. Proposed cyclization mechanism of cyathane diterpenes from GGPP. The black solid and dotted arrows from $\mathbf{C}^+$ to $\mathbf{D}^+$ represent the concerted 1,2-alkyl shift and 10,14-cyclization, respectively.

resolution EIMS *m*/*z* 272.2505), supporting a molecular formula of $C_{20}H_{32}$ and a diterpene with five degrees of unsaturation. The NMR spectra of **1** (Table S2 and Figures S5−S13) revealed two alkenes with three olefinic protons, four methyl groups, seven methylene carbons, three methine carbons, and two sp^3 quaternary carbons. $^1H-^{13}C$ HSQC correlations between δ_H 4.58 and 4.67 ppm with δ_C 108.9 ppm supported the presence of an exomethylene. $^1H-^1H$-COSY revealed two small spin systems (H-7/H-8 and H-13/H-14) and a third larger system (H-1/H-2/H-3/H-4/H-5/H-10/H-11). HMBC correlations connected the three spin systems and placed an isopropenyl moiety at C-3, forming the 5/6/7-tricyclic cyathane skeleton (Figure S9). Supported by 2D NOESY correlations, the H-4, H-5, Me-16, and M-17 on the cyclohexyl ring were all axially oriented: Me-16/H-7_{eq}, Me-17/H-1_b, Me-17/H-2_b, Me-17/H-3, H-2_b/H-3, and Me-17/H-7_{ax}. The NOESY crosspeaks for H-19_b/Me-16, H-19_b/H-10_a, and H-3/H-10_b also supported that the isopropenyl moiety at C-3 and Me-17 are on opposite sides of the cyclopentyl ring. There was some uncertainty in the assignment of the relative configuration due to overlap of the H-4 and H-5 signals; however, the absolute configuration of **1** was confirmed by VCD as 3*R*,4*R*,5*R*,6*S*,9*R* (Figure S14).

3-*epi*-Cyatha-12,18-diene (**2**), a new diterpene, was produced by SpuTS from the myxobacterium *P. spumosum* (Figure 3). The GC-MS and NMR data of **2** (Table S3 and Figures S15−S24) revealed identical molecular weights, spin systems and HMBC correlations with those seen in **1**, with small variations in chemical shifts, suggesting that **2** was a diastereomer of **1**. As with **1**, NOESY correlations of **2** supported that both ring bridgeheads were *trans* fused, but crosspeaks for H-19_a/Me-17, H-19_a/H-5, and H-19_a/H-7_{ax} supported that the isopropenyl moiety at C-3 was oppositely orientated. Thus, the relative configuration of **2** was assigned as 3*S**,4*R**,5*R**,6*S**,9*R**. Both **1** and **2** are the first examples of cyathanes in bacteria; there are no known bacterial NPs bearing this diterpene core. Diterpenoids from myxobacteria are extremely rare and we only recently discovered the first canonical diTS from *Melittangium boletus*[8,27] and therefore the characterization of SpuTS is another welcome addition to the terpenoid biosynthetic capabilities of myxobacteria.

Isopseudolaratriene (**3**), a 5/7-bicyclic diterpene with a prenyl tail, was produced by HarTS from *A. harenae* (Figure 3). The GC-MS of **3** showed a molecular ion peak at *m*/*z* 272.2505 (Figure S25) supporting a molecular formula of $C_{20}H_{32}$ and a diterpene with five degrees of unsaturation. The NMR spectra of **3** (Table S4 and Figures S26−S35) revealed three alkenes with two olefinic protons, five methyl groups, seven methylene carbons, one methine carbon, and one sp^3 quaternary carbon. Along with the four small spin systems seen by $^1H-^1H$-COSY (H-14/H-13/H-12, H-9/H-8, H-6/H-5/H-4, and H-2/H-1), HMBC correlations (Figure S29) supported a 5/7-bicyclic daucadiene skeleton[28] with an additional prenyl tail. The same skeleton, pseudolaratriene, was isolated from an unusual (but not UbiA-type) monofunctional diTS from the golden larch tree and is responsible for beginning the biosynthesis of the microtubule-destabilizing pseudolaric acids.[29] A *trans* fusion of the two rings in **3** was supported by the lack of 1D or 2D NOESY correlations between H-6 and Me-19 (Figures S31−S35). VCD analysis of **3** confirmed its absolute configuration as 6*S*,7*S* (Figure S36).

(+)-Axinyssene (**4**), a known monocyclic diterpene, was isolated from AriTS from *A. arida* (Figure 3). The GC-MS and NMR of **4** (Table S5 and Figures S37−S39) matched previously reported literature.[16] VCD analysis confirmed the absolute configuration of C4 as 4*S* (Figure S40) and thus matching (+)-axinyssene, a previously isolated enzymatic product of the myxobacterial UbiA TS CysTC2.[16] AriTS is found adjacent to the BGC responsible for producing the aridacins (Figure 2B), 6/7/5-tricyclic and highly oxidized diterpenoids, but does not have a role in their biosynthesis.[30]

Diterpenes **1**−**4**, along with lydicene (**5**), are all biosynthetically related via a single cyclization mechanism and supported by DFT studies (Figure 4).[16,31,32] A 1,6-ring (GGPP numbering) closure of the isomerized form of GGPP, geranyllinanyl diphosphate, first leads to the monocyclic intermediate $\mathbf{B}^+$, deprotonation of which yields **4**. The isolation of **3** supports the 5/7-bicyclic intermediate $\mathbf{C}^+$, which arises from expansion of the 6-membered ring of $\mathbf{B}^+$ via a 1,2-alkyl shift and 6,10-ring closure, likely to be a concerted step.[31,32] Next, a 1,2-alkyl shift and subsequent 10,14-cyclization provides the 15-cyathanyl cation ($\mathbf{D}^+$). Direct deprotonation of $\mathbf{D}^+$ yields **1** and **2**; however, the preceding 10,14-cyclization must be stereoselectively controlled by AduTS and SpuTS to set the respective stereocenters at C-3. The fungal cyatha-3,12-diene (**6**) is proposed to form after a 1,2-hydride shift and deprotonation at C-4 (cyathane numbering).[16] Finally, **5** is proposed to arise after another 1,2-alkyl shift to form the 6/6/7 skeleton of $\mathbf{E}^+$ and final deprotonation.

https://doi.org/10.1021/acscatal.5c04650
ACS Catal. 2025, 15, 16873−16881

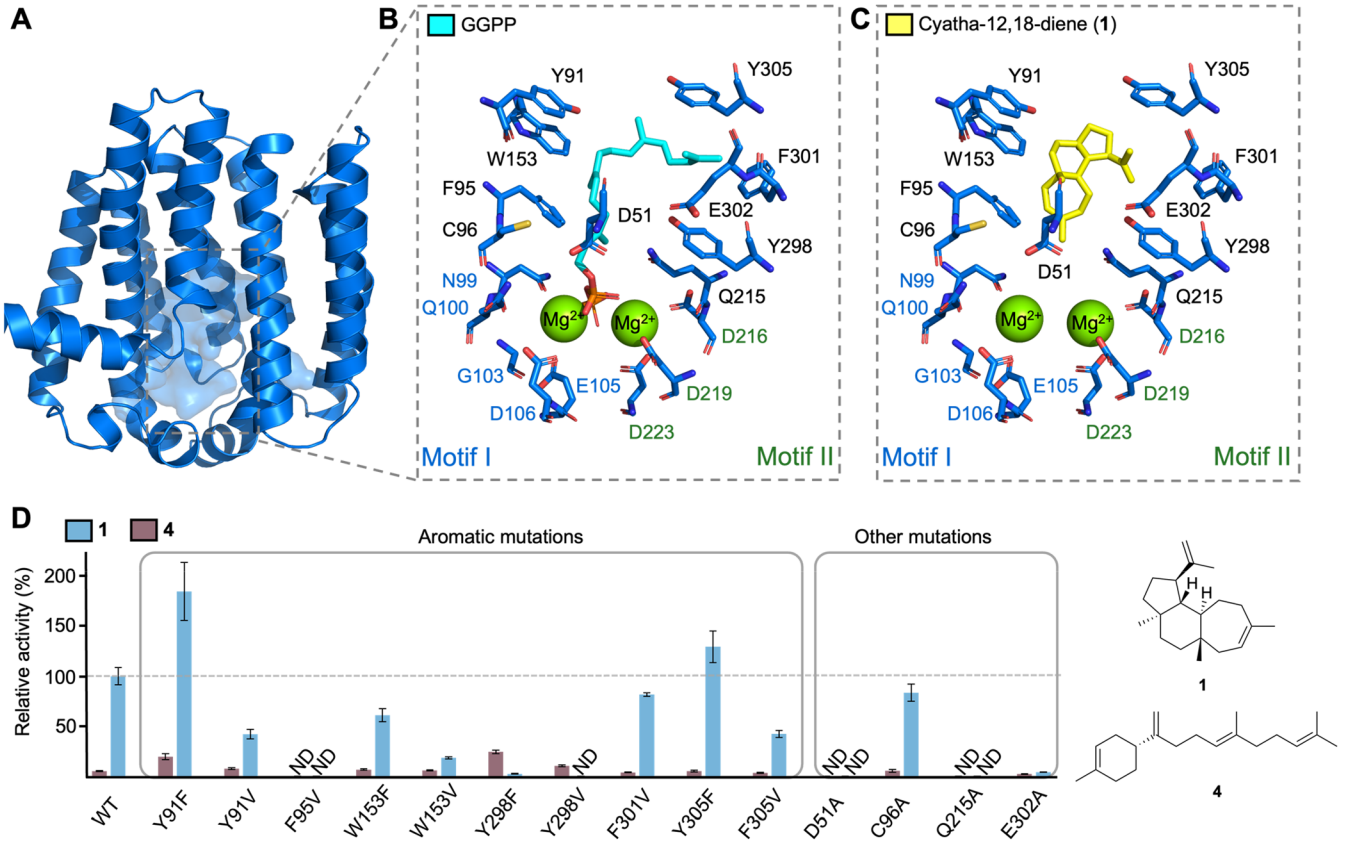

Figure 5. Structural and mutational analysis of AduTS. (A) AlphaFold3 model of AduTS. (B, C) AduTS active site displaying key active-site residues (sticks) with a docked model of GGPP (B) or **1** (C). Mg^{2+} ions (green spheres) were modeled in with AlphaFold3. (D) Relative cyclization activities of AduTS and mutants forming **1** or **4**. ND denotes product not detected.

Mutagenesis Reveals Catalytically Important Residues in the UbiA-like TS AduTS. When investigating TSs, it is common to perform site-directed mutagenesis as perturbations of the active site pockets often alter product distributions due to changes in the shape of the contour or how carbocations are stabilized throughout the mechanism.[1,2,4] However, no substantial mutagenesis experiments with UbiA TSs have been performed, perhaps due to challenges with these membrane-bound enzymes. We were interested in how UbiA TSs behave when their active sites are changed and set out to gain a better understanding of how the bacterial cyathane TSs control their reactions.

First, a multiple sequence alignment of the previously characterized StlTC, CysTC2, and the newly discovered bacterial UbiA diTSs was performed to identify highly conserved residues (Figure S41). The Mg^{2+}-binding acidic motifs, NQxxG/AxxED (motif I) and DxxDxxxD (motif II) were absolutely conserved in all seven enzymes. Aromatic residues F62, Y93, W153, W187, W198, W200, aliphatic residues P112, P115, G125, G145, G178, L183, A186, P192, P232, G236, P252, and polar residues E40, K111, R114, R124, R129, R228, T230, R241 were all absolutely conserved (Figure S41). Aromaticity was highly conserved at position 91, with Phe in AriTS, HarTS, and CysTC2 and Tyr in AduTS, SpuTS, AciTS, and StlTC. Interestingly, the TSs with Y91 make the cyathane tricyclic skeletons while those with F91 produce either the mono- or bicyclic structures, suggesting this position may help to navigate the cyclization pathway either via cation stabilization or as a base for deprotonation of the cyathanes. ConSurf[32] facilitated deeper analysis of AduTS-like UbiAs, further supporting the structural/functional importance of several aromatic, aliphatic, and polar residues largely concentrated around the active site (Figures S42 and S43). An AlphaFold3[33] model of AduTS was analyzed with ligand docking to further probe residues of interest. The "bottom" of the pocket, which opens to the cytoplasmic side of the membrane, harbors motifs I and II on opposing sides (Figure 5). Deeper in the cavity of AduTS is the hydrophobic pocket lined with aromatic (Y91, F95, W153, F301, and Y305) and aliphatic (A54, G55, L92, I175, G176, G178, V179, M182, V208, and I212) residues (Figure 5). Four additional polar residues (D51, C96, Q215, and E302) protrude into the active site. Docking of **1** into the model of AduTS placed the isopropenyl moiety near Y298 (3.5 Å), suggesting that this residue may be involved in quenching the final cationic intermediate.

We constructed 14 single point variants of AduTS and screened them using our *E. coli* system to investigate their functional importance (Figures 5 and S45). Many mutations targeting aromatic residues reduced the overall production of diterpene products **1** and **4**, but **1** was still the major product with no detectable bicyclic diterpenes. Variants D51A, F95V, and Q215A showed complete loss of cyclase activity; however, it is unknown if this is due to disruption of catalysis or improper protein folding. The variants Y91F and Y305F, however, increased the relative production of **1** compared with native AduTS. Changes to Y298 (Y298F and Y298V) swapped the major diterpene from **1** to **4**, indicating Y298 plays a key role in guiding the pathway toward the cyathanes. However, we cannot determine if Y298 is the catalytic base as trace

https://doi.org/10.1021/acscatal.5c04650
ACS Catal. 2025, 15, 16873−16881

amounts of **1** were still seen when the hydroxy group of Y298 was removed. Diterpene production was completely abolished in F95 V, D51A, and Q215A, and only trace amounts of **1** and **4** were seen in the E302A variant. F95, D51, Q215, and E302 are all highly conserved among UbiA TSs (Figures S42 and S43), suggesting that they play important roles in maintaining the structural integrity or chemical environment of the active site pocket. Electrostatic surface potential maps of AduTS active site mutants reveal that most of the variants introduce only modest changes to the pocket; however, D51A, Q215A, and E302A lead to an appreciable change in acidic/basic character (Figure S44), which clearly impacts catalysis. Because our assays were performed in *E. coli*, we are unable to rule out if any of the mutations that abolish activity are solely due to improper folding of AduTS. This work showcases that UbiA TSs are amenable to the introduction of active site mutations for the purpose of biochemical and mechanistic investigations, which will serve to bridge the gap in our understanding of UbiA TSs moving forward. One such question is the structural basis of stereochemical control that AduTS and SpuTS use to biosynthesize C-3 epimers of cyathane. AduTS and SpuTS share 46% sequence identity (Figure S41) and structural models of AduTS and SpuTS reveal that the shapes of the pockets are very similar but have at least eight residue differences located deep in the hydrophobic pocket (Figure S46) that may contribute to altering the conformation of $\mathbf{C}^+$ prior to tricyclic formation.

CONCLUSIONS

UbiA-type TSs remain a significantly understudied family of enzymes in NP biosynthesis. The discovery of the first bacterial cyathane TSs highlights the potential that this subtype of TSs has in forming diverse and stereochemically distinct scaffolds for downstream functionalization. Cyathane-derived NPs, with >180 examples from fungi and >40 others from sponges, liverworts, and ferns, wield a wide range of biological activities.[34,35] Their properties have sparked numerous total syntheses to access these molecules for drug development. With this discovery, it is now reasonable to imagine that bacteria make their own versions of cyathane-derived NPs that can be exploited for chemical and biological studies. We also expect that UbiA TSs are capable of producing numerous and diverse hydrocarbon skeletons, and more BGCs encoding UbiAs across all types of bacteria and other organisms should be prioritized for NP discovery efforts.

MATERIALS AND METHODS

Bacterial Strains, Plasmids, and Chemicals. Strains, plasmids, and PCR primers used in this study are listed in Tables S6−S8. *E. coli* Turbo cells were used for general cloning. Enzymes and reagents for general cloning procedures including Q5 high-fidelity DNA polymerase, restriction enzymes, buffers, and dNTPs were purchased from NEB and used according to the manufacturer's suggested protocols. Omega Bio-Tek gel extraction and plasmid isolation kits were used for the purification of digested plasmids, PCR fragments, and plasmids harboring the desired gene inserts. All media components, chemicals, and solvents were purchased at high quality from various commercial suppliers.

General Experimental Procedures. All 1D (^{1}H and ^{13}C) and 2D (^{1}H−^{13}C HSQC, ^{1}H−^{1}H-COSY, ^{1}H−^{13}C HMBC) NMR experiments were performed in $CDCl_3$ on either a Bruker AVANCE III Ultrashield 600, a Bruker AVANCE III HD 600 equipped with a 5 mm TXI CryoProbe. All NMR chemical shifts in $CDCl_3$ were referenced to residual $CHCl_3$ at 7.26 ppm for 1H or 77.00 ppm for ^{13}C. For preparative reversed-phase chromatography, an Agilent 1260 Infinity LC system equipped with an Agilent Eclipse XDB-C18 column (250 mm × 21.2 mm, 7 μm) was used. TLC was performed with 0.25 mm silica gel plates (60 F_{254}) using short-wave UV light to visualize, and $KMnO_4$ and heat as developing agents. Optical rotations were measured using a JASCO P-2000 polarimeter. VCD data were collected on a ChiralIR-2XTM Dual PEM FT-VCD spectrometer (BioTools, Inc., West Palm Beach, FL).

General Cloning. All genes encoding bacterial TSs screened in this study were synthesized by the U.S. Department of Energy Joint Genome Institute as part of a User Proposal for Functional Genomics (part of proposal: 10.46936/10.25585/60008123). Genes were codon-optimized for *E. coli* and cloned into pET45b via Gibson assembly. The primers described in Table S3 were used to amplify genes from plasmid DNA using Q5 high-fidelity DNA polymerase and cloned into *Nco*I/*Bst*BI double-digested pET45b via T5 exonuclease-dependent assembly (TEDA).[36] Plasmid isolation was conducted from DNA gel extraction using plasmid mini prep kits from Omega Bio-Tek and plasmids were sequenced by Genewiz to confirm introduction of correct mutations.

Terpene Synthase Screen. Plasmids harboring UbiA TS genes in pET45b were isolated using *E. coli* NEB Turbo grown in lysogeny broth (LB) with ampicillin (100 mg L^{-1}) following manufacturer's protocols. Each plasmid was individually transformed into *E. coli* BL21 Star (DE3) competent cells already containing pJR1064b, a pCDF-Duet vector harboring genes that produce GGPP in vivo via an alternative isoprenoid precursor pathway.[25] Transformants were cultivated in lysogeny broth (LB) containing ampicillin (100 mg L^{-1}) and streptomycin (50 mg L^{-1}). The cells were cultured overnight were subsequently inoculated into 50 mL of Terrific Broth (TB) media at 37 °C with shaking at 250 rpm until reaching an optical density at 600 nm (OD_{600}) of 1.0. Isopropyl β-D-1-thiogalactopyranoside (IPTG, 0.5 mM final concentration) and isoprenol (4 mM, final concentration) were added to the culture and the culture was shaken at 250 rpm for 24 h at 28 °C. For analysis, 1 mL of culture was extracted using 0.5 mL of acetonitrile, saturated with solid NaCl, after vigorous vortexing and centrifugation at 15,600 rpm for 5 min. The organic layer, containing the terpene products of each TS, was initially analyzed by analytical HPLC. For HPLC analysis, products were detected at 210 nm using a linear gradient with flow rate of 1 mL min^{-1}: 5% CH_3CN in H2O for 5 min, followed by a 20 min solvent gradient from 5−98% CH_3CN in H_2O, and ending with a 25 min hold at 98% CH_3CN in H_2O.

GC-MS Analysis. GC-MS analysis of all terpenes for exact mass and Kovats retention index (RI) calculations were run using a Thermo Scientific Orbitrap Exploris spectrometer with an Rxi-5MS column (Restek Corp, 30 m × 0.25 mm i.d. and 0.251 μm film). GC-MS data used to generate chromatograms of mass spectra were obtained for all compounds using a Thermo Scientific Trace 1610 Gas Chromatograph ISQ 7610 Single Quadrupole Mass Spectrometer with an Rxi-5MS column (Restek Corp, 30 m × 0.25 mm i.d. and 0.25 μm film).

For GC-MS analysis, purified diterpenes and crude cell extracts were dissolved in hexanes or acetonitrile at a concentration of approximately 1 mg mL^{-1}. The source,

https://doi.org/10.1021/acscatal.5c04650
ACS Catal. 2025, 15, 16873−16881

transfer line, and injection port were set to 250 °C, 280 °C, and 250 °C, respectively, and the carrier gas flow rate was set at 1.2 mL min^{-1}. The compounds were measured with an electron ionization of 70 eV and mass scan range was from m/z 30−500 @ 30,000 resolution with a temperature gradient as follows: 50 °C (0−3 min), ramp to 280 °C @ 10 °C min^{-1} (hold 5 min). RI values were calculated for all products in this study using the GC-MS conditions above in comparison with C7−C30 saturated alkanes (Sigma). To obtain spectra for chromatograms, the source, transfer line, and injection port were set to 300 °C, 280 °C, and 300 °C, respectively, and the carrier gas flow rate was set at 1.0 mL min^{-1}. The compounds were measured with an electron ionization of 70 eV and mass scan range was from m/z 45−450 at unit resolution with a temperature gradient as follows: after a 10 s dwell time prior to injection, 50 °C (0−1 min), ramp to 300 °C @ 15 °C min^{-1} (hold 5 min).

VCD Measurements and Calculations. See Supporting Information (SI) for detailed methods. Briefly, **1**, **3**, and **4** were individually dissolved in $CDCl_3$, transferred to a liquid IR cell, and IR and VCD data were collected. DFT-calculated IR and VCD spectra of arbitrary enantiomers were obtained using Gaussian.[37] Quantitative comparisons of the experimental and DFT spectra resulted in very high confidence level assignments (CompareVOA, BioTools, Inc., Jupiter, FL).[38,39]

Bioinformatics. See SI for detailed methods. Briefly, phylogenetic analysis was conducted using MEGA12 (ref 40) and visualized using iTOL.[41] Sequence similarity and genome neighborhood networks were generated using the Enzyme Function Initiative webtools.[23] Docking was performed using AutoDock Vina.[42]

Spectroscopic Data of Isolated Diterpenes. cyatha-12,18-diene (**1**): clear oil, RI = 1904; R_f = 0.85 (hexanes); $[\alpha]_D^{22}$ = −50.34° (c 0.89, CH_2Cl_2); IR (cm^{-1}): 1645, 1620, 1435, 1425, 1360, 1240, 1220, 1160, 1100, 1020; UV (acetonitrile:water = 49:1): λ_{max} = 210 nm; ^1H and ^{13}C NMR data, see Table S2 and Figures S5−S13; HR-EIMS = 272.2505.

3-epi-cyatha-12,18-diene (**2**): clear oil, RI = 1969; R_f = 0.88 (hexanes); $[\alpha]_D^{22}$ = +43.48° (c 0.42, CH_2Cl_2); IR (cm^{-1}): 1646, 1453, 1379, 1217, 1146, 1071, 1013, 986; UV (acetonitrile:water = 49:1): λ_{max} = 210 nm; ^1H and ^{13}C NMR data, see Table S3 and Figures S16−S24; HR-EIMS = 272.2501.

isopseudolaratriene (**3**): clear oil, RI = 2008; R_f = 0.87 (hexanes); $[\alpha]_D^{22}$ = +5.66° (c 0.95, CH_2Cl_2); IR (cm^{-1}): 1670, 1640, 1565, 1440, 1355, 1320, 1250, 1100, 1060, 970; UV (acetonitrile:water = 49:1): λ_{max} = 210 nm; ^1H and ^{13}C NMR data, see Table S4 and Figures S26−S35; EIMS = 272.2505.

(+)-axinyssene (**4**): clear oil, RI = 1998; R_f = 0.72 (hexanes); $[\alpha]_D^{22}$ = −28.56° (c 7.4, CH_2Cl_2); IR (cm^{-1}): 1640, 1620, 1445, 1430, 1360, 1310, 1280, 1145, 1100, 1045, 1020, 975; UV (acetonitrile:water = 49:1): λ_{max} = 210 nm; ^1H and ^{13}C NMR data, see Table S5 and Figures S38 and S39; HR-EIMS = 272.2498.

■ ASSOCIATED CONTENT

Supporting Information

The Supporting Information is available free of charge at https://pubs.acs.org/doi/10.1021/acscatal.5c04650.

Methods, data, and references; UbiA TS and accession numbers (Table S1); summary of NMR data for **1**−**4** (Tables S2−S5); strains, plasmids, and primers (Tables S6−S8); bioinformatics of bacterial UbiAs (Figures S1−S3); spectroscopic data for **1**−**4** (Figures S4−S40); protein sequence and structural model analyses (Figures S41−S46); GC-MS chromatograms of AduTS variants (PDF)

■ AUTHOR INFORMATION

Corresponding Author

Jeffrey D. Rudolf − *Department of Chemistry, University of Florida, Gainesville, Florida 32611-7011, United States;* orcid.org/0000-0003-2718-9651; Email: jrudolf@chem.ufl.edu

Authors

Tyler A. Alsup − *Department of Chemistry, University of Florida, Gainesville, Florida 32611-7011, United States*

Diana P. Łomowska-Keehner − *Department of Chemistry, University of Florida, Gainesville, Florida 32611-7011, United States*

Melvin Osei Opoku − *Department of Chemistry, University of Florida, Gainesville, Florida 32611-7011, United States*

Zining Li − *Department of Chemistry, University of Florida, Gainesville, Florida 32611-7011, United States;* Present Address: Department of Biopharmaceutics, West China School of Pharmacy, Sichuan University, Chengdu 610041, PR China; Key Laboratory of Drug-Targeting and Drug Delivery System of the Education Ministry and Sichuan Province, Sichuan Engineering Laboratory for Plant-Sourced Drug and Sichuan Research Center for Drug Precision Industrial Technology, West China School of Pharmacy, Sichuan University, Chengdu 610041, China; orcid.org/0000-0002-6921-8417

Caitlin A. McCadden − *Department of Chemistry, University of Florida, Gainesville, Florida 32611-7011, United States*

Tracy Qu − *Department of Chemistry, University of Florida, Gainesville, Florida 32611-7011, United States*

Glen Gillia − *Department of Chemistry, University of Florida, Gainesville, Florida 32611-7011, United States*

Jordan Nafie − *BioTools, Inc., West Palm Beach, Florida 33407, United States*

Complete contact information is available at: https://pubs.acs.org/10.1021/acscatal.5c04650

Notes

The authors declare no competing financial interest.

■ ACKNOWLEDGMENTS

This work is supported in part by the National Institutes of Health Grant R35 GM142574 and the University of Florida. The synthesis of the TS genes (part of proposal: 10.46936/10.25585/60008123) was conducted by the U.S. Department of Energy Joint Genome Institute, a DOE Office of Science User Facility, operated under contract no. DE-AC02-05CH11231. T.A.A. was supported in part by a Chemistry-Biology Interface Research Training Program Grant T32 GM136583. We thank the University of Florida Mass Spectrometry Research and Education Center, which is supported by the NIH (S10 OD021758-01A1) and Jodie Johnson and Katie Heiden for GC-MS support. We acknowledge both the University of Florida Center for Nuclear Magnetic Resonance Spectroscopy and the University of

Florida McKnight Brain Institute at the National High Magnetic Field Laboratory's Advanced Magnetic Resonance Imaging and Spectroscopy (AMRIS) Facility, which is supported by the US NSF Cooperative Agreement No. DMR-1644779 and the State of Florida, for NMR support. We thank James Rocca and Ion Ghiviriga for their excellent NMR support.

REFERENCES

(1) Christianson, D. W. Structural and chemical biology of terpenoid cyclases. *Chem. Rev.* **2017**, *117*, 11570−11648.
(2) Pan, X.; Rudolf, J. D.; Dong, L. Bin. Class II terpene cyclases: structures, mechanisms, and engineering. *Nat. Prod. Rep.* **2024**, *41*, 402−433.
(3) Rudolf, J. D.; Alsup, T. A.; Xu, B.; Li, Z. Bacterial terpenome. *Nat. Prod. Rep.* **2021**, *38*, 905−980.
(4) Dickschat, J. S. Bacterial terpene cyclases. *Nat. Prod. Rep.* **2016**, *33*, 87−110.
(5) Avalos, M.; Garbeva, P.; Vader, L.; Van Wezel, G. P.; Dickschat, J. S.; Ulanova, D. Biosynthesis, evolution and ecology of microbial terpenoids. *Nat. Prod. Rep.* **2022**, *39*, 249−272.
(6) Van Santen, J. A.; Poynton, E. F.; Iskakova, D.; Mcmann, E.; Alsup, T. A.; Clark, T. N.; Fergusson, C. H.; Fewer, D. P.; Hughes, A. H.; McCadden, C. A.; Parra, J.; et al. The Natural Products Atlas 2.0: a database of microbially-derived natural products. *Nucleic Acids Res.* **2022**, *50*, D1317−D1323.
(7) Cane, D. E.; Ikeda, H. Exploration and mining of the bacterial terpenome. *Acc. Chem. Res.* **2012**, *45*, 463−472.
(8) Wei, X.; Ning, W.; McCadden, C. A.; Alsup, T. A.; Li, Z.; Łomowska-Keehner, D. P.; Nafie, J.; Qu, T.; Opoku, M. O.; Gillia, G. R.; Xu, B.; Icenhour, D. G.; Rudolf, J. D. Exploring and expanding the natural chemical space of bacterial diterpenes. *Nat. Commun.* **2025**, *16*, No. 3721.
(9) Yamada, Y.; Kuzuyama, T.; Komatsu, M.; Shin-ya, K.; Omura, S.; Cane, D. E.; Ikeda, H. Terpene synthases are widely distributed in bacteria. *Proc. Natl. Acad. Sci. U.S.A.* **2015**, *112*, 857−862.
(10) Rudolf, J. D.; Chang, C. Y. Terpene synthases in disguise: enzymology, structure, and opportunities of non-canonical terpene synthases. *Nat. Prod. Rep.* **2020**, *37*, 425−463.
(11) Li, W. Bringing bioactive compounds into membranes: the UbiA superfamily of intramembrane aromatic prenyltransferases. *Trends Biochem. Sci.* **2016**, *41*, 356−370.
(12) Cheng, W.; Li, W. Structural insights into ubiquinone biosynthesis in membranes. *Science* **2014**, *343*, 878−881.
(13) Smanski, M. J.; Yu, Z.; Casper, J.; Lin, S.; Peterson, R. M.; Chen, Y.; Wendt-Pienkowski, E.; Rajski, S. R.; Shen, B. Dedicated *ent*-kaurene and *ent*-atiserene synthases for platensimycin and platencin biosynthesis. *Proc. Natl. Acad. Sci. U.S.A.* **2011**, *108*, 13498−13503.
(14) Luo, P.; Lv, J. M.; Xie, Y. F.; Xiao, L. Y.; Qin, S. Y.; Chen, G. D.; Luo, X. Z.; Hu, D.; Gao, H. Discovery and characterization of a novel sub-group of UbiA-type terpene cyclases with a distinct motif I. *Org. Chem. Front.* **2022**, *9*, 3057−3060.
(15) Lin, H. C.; Chooi, Y. H.; Dhingra, S.; Xu, W.; Calvo, A. M.; Tang, Y. The fumagillin biosynthetic gene cluster in *Aspergillus fumigatus* encodes a cryptic terpene cyclase Involved in the Formation of *β-trans*-bergamotene. *J. Am. Chem. Soc.* **2013**, *135*, 4616−4619.
(16) Yang, Y.; Zhang, S.; Ma, K.; Xu, Y.; Tao, Q.; Chen, Y.; Chen, J.; Guo, S.; Ren, J.; Wang, W.; Tao, Y.; Yin, W.; Liu, H. Discovery and characterization of a new family of diterpene cyclases in bacteria and fungi. *Angew. Chem., Int. Ed.* **2017**, *129*, 4827−4830.
(17) Yang, Y.; Zhang, Y.; Zhang, S.; Chen, Q.; Ma, K.; Bao, L.; Tao, Y.; Yin, W.; Wang, G.; Liu, H. Identification and characterization of a membrane-bound sesterterpene cyclase from *Streptomyces somaliensis*. *J. Nat. Prod.* **2018**, *81*, 1089−1092.
(18) Zdouc, M. M.; Blin, K.; Louwen, N. L. L.; Navarro, J.; Loureiro, C.; Bader, C. D.; Bailey, C. B.; Barra, L.; Booth, T. J.; Bozhüyük, K. A. J.; et al. MIBiG 4.0: Advancing biosynthetic gene cluster curation through global collaboration. *Nucleic Acids Res.* **2025**, *53*, D678−D690.
(19) Alsup, T. A.; Opoku, M. O.; Rudolf, J. D. Characterization of UbiA terpene synthases with a precursor overproduction system in *Escherichia coli*. *Methods Enzymol.* **2024**, *699*, 395−417.
(20) van der Meij, A.; Worsley, S. F.; Hutchings, M. I.; van Wezel, G. P. Chemical ecology of antibiotic production by actinomycetes. *FEMS Microbiol. Rev.* **2017**, *41*, 392−416.
(21) Actinomycetes: Still a source of novel antibiotics. *Nat. Prod. Rep.* **2017**, *34*, 1203−1232.
(22) Hoshino, Y.; Villanueva, L. Four billion years of microbial terpenome evolution. *FEMS Microbiol. Rev.* **2023**, *47*, No. fuad027.
(23) Oberg, N.; Zallot, R.; Gerlt, J. A. EFI-EST, EFI-GNT, and EFI-CGFP: Enzyme Function Initiative (EFI) web resource for genomic enzymology tools. *J. Mol. Biol.* **2023**, *435*, No. 168018.
(24) Rudolf, J. D.; Chang, C. Y.; Ma, M.; Shen, B. Cytochromes P450 for natural product biosynthesis in *Streptomyces*: sequence, structure, and function. *Nat. Prod. Rep.* **2017**, *34*, 1141−1172.
(25) Li, Z.; Xu, B.; Kojasoy, V.; Ortega, T.; Adpressa, D. A.; Ning, W.; Wei, X.; Liu, J.; Tantillo, D. J.; Loesgen, S.; Rudolf, J. D. First *trans*-eunicellane terpene synthase in bacteria. *Chem.* **2023**, *9*, 698−708.
(26) Cassidy, M. P.; Ghisalberti, E. L. New terpene hydrocarbons from the sponge Higginsia sp. *J. Nat. Prod.* **1993**, *56*, 1190−1193.
(27) Wei, X.; DeSnoo, W.; Li, Z.; Ning, W.; Kong, W. Y.; Nafie, J.; Tantillo, D. J.; Rudolf, J. D. Avoidance of secondary carbocations, Unusual deprotonation, and nonstatistical dynamic effects in the cyclization mechanism of tetraisoquinane. *J. Am. Chem. Soc.* **2025**, *147*, 16293−16300.
(28) Yan, Y.; Liu, Q.; Zang, X.; Yuan, S.; Bat-Erdene, U.; Ngyuen, C.; Gan, J.; Zhou, J.; Jaconsen, S. E.; Tang, Y. Resistance-gene-directed discovery of a natural-product herbicide with a new mode of action. *Nature* **2018**, *559*, 415−418.
(29) Mafu, S.; Karunanithi, P. S.; Palazzo, T. A.; Harrod, B. L.; Rodriguez, S. M.; Mollhoff, I. N.; O'Brien, T. E.; Tong, S.; Fiehn, O.; Tantillo, D. J.; Bohlmann, J.; Zerbe, P. Biosynthesis of the microtubule-destabilizing diterpene pseudolaric acid B from Golden Larch involves an unusual diterpene synthase. *Proc. Natl. Acad. Sci. U.S.A.* **2017**, *114*, 974−979.
(30) Wang, Z.; Yang, Q.; He, J.; Li, H.; Pan, X.; Li, Z.; Xu, H.-M.; Rudolf, J. D.; Tantillo, D. J.; Dong, L.-B. Cytochrome P450-mediated cyclization in eunicellane-derived diterpenoid biosynthesis. *Angew. Chem., Int. Ed.* **2023**, *62*, No. e202312490.
(31) Sato, H.; Li, B.-X.; Takagi, T.; Wang, C.; Miyamoto, K.; Uchiyama, M. DFT study on the biosynthesis of verrucosane diterpenoids and mangicol sesterterpenoids: Involvement of secondary-carbocation-free reaction cascades. *JACS Au* **2021**, *1*, 1231−1239.
(32) (a) Xu, K.; Xie, Z.; Kang, X.; Wu, R. Probing intermediate folding patterns determined the carbon skeleton construction mechanism of cyathane diterpene. *Phys. Chem. Chem. Phys.* **2025**, *27*, 11887−11897. (b) Ashkenazy, H.; Abadi, S.; Martz, E.; Chay, O.; Mayrose, I.; Pupko, T.; Ben-Tal, N. ConSurf 2016: An improved methodology to estimate and visualize evolutionary conservation in macromolecules. *Nucleic Acids Res.* **2016**, *44*, W344−W350.
(33) Abramson, J.; Adler, J.; Dunger, J.; Evans, R.; Green, T.; Pritzel, A.; Ronneberger, O.; Willmore, L.; Ballard, A. J.; Bambrick, J.; et al. Accurate structure prediction of biomolecular interactions with AlphaFold 3. *Nature* **2024**, *630*, 493−500.
(34) Bailly, C.; Gao, J. M. Erinacine A and related cyathane diterpenoids: Molecular diversity and mechanisms underlying their neuroprotection and anticancer activities. *Pharmacol. Res.* **2020**, *159*, No. 104953.
(35) Dictionary of Natural Products. http://dnp.chemnetbase.com. accessed May 2025.
(36) Xia, Y.; Li, K.; Li, J.; Wang, T.; Gu, L.; Xun, L. T5 exonuclease-dependent assembly offers a low-cost method for efficient cloning and site-directed mutagenesis. *Nucleic Acids Res.* **2019**, *47*, No. e15.

https://doi.org/10.1021/acscatal.5c04650
ACS Catal. 2025, 15, 16873−16881

(37) Frisch, M.; Trucks, G. W.; Schlegel, H. B.; Scuseria, G. E.; Robb, M. A.; Cheeseman, J. R.; Scalmani, G.; Barone, V.; Petersson, G. A.; Nakatsuji, H.et al. *Gaussian 09*, Revision E.01; Gaussian Inc.: Wallingford CT, 2009.
(38) He, Y.; Bo, W.; Dukor, R. K.; Nafie, L. A. Determination of absolute configuration of chiral molecules using vibrational optical activity: a review. *Appl. Spectrosc.* **2011**, *65*, 699−723.
(39) Polavarapu, P. L.; Covington, C. L. Comparison of experimental and calculated chiroptical spectra for chiral molecular structure determination. *Chirality* **2014**, *26*, 539−552.
(40) Kumar, S.; Stecher, G.; Suleski, M.; Sanderford, M.; Sharma, S.; Tamura, K. MEGA12: Molecular Evolutionary Genetic Analysis version 12 for adaptive and green computing. *Mol. Biol. Evol.* **2024**, *41*, No. msae263.
(41) Letunic, I.; Bork, P. Interactive Tree of Life (iTOL) v6: Recent updates to the phylogenetic tree display and annotation tool. *Nucleic Acids Res.* **2024**, *52*, W78−W82.
(42) Trott, O.; Olson, A. J. AutoDock Vina: Improving the speed and accuracy of docking with a new scoring function, efficient optimization, and multithreading. *J. Comput. Chem.* **2010**, *31*, 455−461.

https://doi.org/10.1021/acscatal.5c04650
ACS Catal. 2025, 15, 16873−16881